Analysis of the Narrowband Interference Effect on OFDM Timing Synchronization

Mohamed Marey and Heidi Steendam, *Senior Member, IEEE*

Abstract—In OFDM systems, the symbol timing synchronization is needed to find an estimate of where the symbol starts. The most popular of the pilot-aided timing estimators is the one proposed by Schmidl and Cox (S&C) ["Robust Frequency and Timing Synchronization for OFDM," *IEEE Transactions on Communications*, vol. 45, no. 12, pp. 1613–1621, Dec. 1997]. Generally, the proper action of the timing estimator may be strongly affected by the presence of disturbances, like narrowband interference (NBI) signals. This paper investigates the effect of NBI signals, which may arise in the OFDM band as the spectrum becomes more crowded, on the timing synchronization for OFDM systems. The performance of the S&C symbol timing synchronizer is evaluated in an analytical way in the presence of narrowband interferers. Also, the probabilities of both missing and false detection of a training sequence are addressed. Further, simulations have been carried out to verify the validity of the approximations in the analysis.

Index Terms—Interference, orthogonal-frequency-division multiplexing (OFDM), symbol timing synchronization, training symbol.

I. INTRODUCTION

ONE of the most challenging issues for future wireless communications is the provision of new spectral resources and the more efficient use of existing frequency bands. Recently, new spectrum management strategies have been proposed [2], [3] which allow two or more systems to share the same frequency band. The broadband very high frequency (B-VHF) project[1] [4], [5] which aims to develop a new integrated broadband VHF system for aeronautical voice and data link communications based on multicarrier (MC) technology, is a good example of an overlay system. In this project, the MC system is intended to share the parts of the VHF spectrum with currently existing narrowband (NB) systems such as voice double side band/amplitude modulation (DSB-AM) signals and VHF digital links. These NB systems are considered as interference to the MC system and limit the effectiveness of the multicarrier system. According to the authors' knowledge, no previous research was done to investigate the effect of these NB signals on the performance of a MC system. In [6],

Coulson investigated the effect of narrowband interference (NBI) on pilot symbol detection and frequency synchronization for OFDM systems; the NBI model in [6] was an unmodulated complex sinusoid. Although this model is an accurate model for different interference sources [7] such as carrier feed-through, baby monitors, and garage doors, this model is not sufficient to describe interference sources with a bandwidth that is larger than a small fraction of the carrier spacing of the MC system. This motivates us to study the effect of digitally modulated NBI signals on the OFDM systems. In [8], we have investigated the effect of digitally modulated NBI signals on frequency ambiguity resolution of OFDM systems. The result of [8] indicates that the performance of the integer frequency estimator is strongly affected by NBI. In this paper, we evaluate the impact of digitally modulated NBI signals on timing synchronization, which is one of the most important parts of the OFDM receiver. The proposed interference model for NBI can also be used to describe the interference in other applications where a MC system has to coexist with NB signals.

In symbol timing synchronization, the main objective is to know when a received OFDM symbol starts. In the case of an ideal channel, the synchronizer must select a timing within the range of the cyclic prefix to avoid intercarrier interference (ICI) and intersymbol interference (ISI) [9]–[11]. Indeed, a timing offset not exceeding the length of the cyclic prefix gives only rise to a carrier-dependent phase rotation [10], which can easily be corrected by the channel equalizer at the FFT outputs. However, a time shift larger than the cyclic prefix will cause the introduction of ICI and ISI. In a dispersive channel, the interval over which the timing may range is reduced as compared to the case of the ideal channel, with an amount equal to the impulse response duration of the channel.

Symbol timing synchronization at the receiver can be achieved by inserting some synchronization symbols at the transmitter as pilot OFDM symbols [1], [12], [13]. These symbols are then picked up by the receiver to synchronize the symbol clock. The most popular of the pilot-aided algorithms is the method proposed by Schmidl and Cox (S&C) [1]. The method relies on searching for a pilot OFDM symbol with two identical halves in time domain. This symbol is generated by transmitting pseudonoise (PN) data symbols at even frequencies, while zeros are used on the odd frequencies. The S&C estimator provides a simple and robust estimation for symbol timing.

In this paper, we investigate the performance of the S&C method in the presence of NBI signals. The paper is organized as follows. In Section II, we describe the OFDM system in the presence of NBI signals. In Section III, the statistical properties of the timing metric of the S&C estimator in the presence of

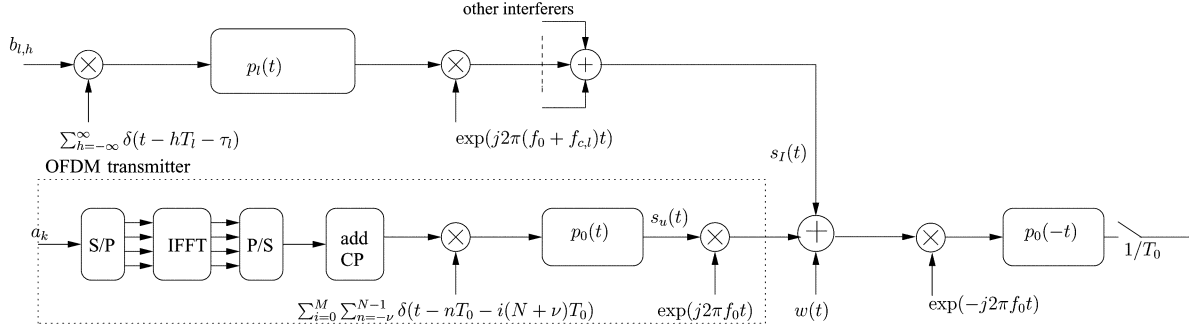[1]B-VHF project website [Online] available: http://www.b-vhf.org

Fig. 1. Block diagram of OFDM system including interfering signals.

interference are derived. The simulation and analytical results are discussed in Section IV. Finally, conclusions are given in Section V.

II. SYSTEM DESCRIPTION

The basic block diagram of the OFDM system and NBI signals is shown in Fig. 1. In the OFDM transmitter, the data stream is grouped in blocks of N_u data symbols. Next, an N-point inverse fast Fourier transform (IFFT) is performed on each data block, where $N > N_u$ and a cyclic prefix of length ν is inserted. The nth time-domain sample of the ith data carrying OFDM block can be written as

$$s^i(n) = \sqrt{\frac{1}{N+\nu}} \sum_{k \in I_u} a_k^i \, e^{j2\pi kn/N} \quad -\nu \leq n \leq N-1 \quad (1)$$

where I_u is the set of N_u carrier indexes and a_k^i is the kth data symbol of the ith OFDM block; data symbols are independently and identically distributed (i.i.d.) with zero mean and variance $E\left[\left|a_k^i\right|^2\right] = E_s$. The M data OFDM blocks are preceded by one OFDM training symbol; the training symbol consists of two identical halves in the time domain. The time-domain samples of the training symbol can be written as in (1), but with the symbols modulated on the odd carriers equal to zero and on even carriers equal to a pseudonoise sequence; the energy per symbol on the even carriers equals ($2E_s$). The time-domain signal of the baseband OFDM signal $s_u(t)$ consists of the concatenation of the two pilot block and the M data OFDM blocks, as follows:

$$s_u(t) = \sum_{i=0}^{M} \sum_{n=-\nu}^{N-1} s^i(n) p_0(t - nT_0 - i(N+\nu)T_0) \quad (2)$$

where $i = 0$ corresponds to the pilot block and $i = 1, \ldots, M$ corresponds to the M data carrying blocks, $p_0(t)$ is the transmit pulse of the OFDM system, and $1/T_0$ is the sample rate. The transmit pulse $p_0(t)$ is assumed to be a square-root-raised cosine filter with roll-off α_0. The baseband signal (2) is upconverted to the radio frequency f_0. At the receiver, the signal is first downconverted, then fed to the matched filter and finally sampled at rate $1/T_0$, resulting in the samples $r_u(mT_0)$. Note that, when the number of carriers N is large, the sample $s^i(n)$ consists of a large number of contributions. Hence, taking into account the
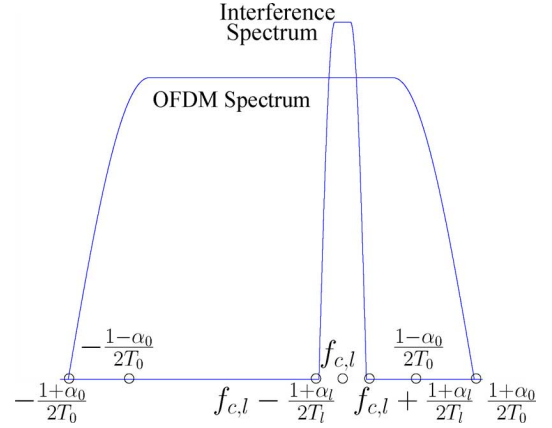

Fig. 2. Spectrum of baseband OFDM and one interfering signal.

central limit theorem, the real and imaginary parts of $s^i(n)$ can be modeled as Gaussian random variables with zero mean and variance σ_s^2 equal to $(E_s \cdot N_u/2)/(N+\nu)$. The OFDM signal is disturbed by additive white Gaussian noise (AWGN) with uncorrelated real and imaginary parts, each having variance σ_n^2. The signal-to-noise ratio (SNR) at the output of the matched filter is defined as σ_s^2/σ_n^2.

Further, the signal is disturbed by narrowband interference residing within the same frequency band as the wideband OFDM signal as shown in Fig. 2. The interfering signal $s_I(t)$ may be modeled as the sum of N_I narrowband interfering signals

$$s_I(t) = \sum_{l=1}^{N_I} s_l(t) \quad (3)$$

where $s_l(t)$ is the lth NBI component

$$s_l(t) = \sum_{h=-\infty}^{\infty} b_{l,h} p_l(t - hT_l - \tau_l) \cdot e^{j2\pi(f_0 + f_{c,l})t} \quad (4)$$

where $b_{l,h}$ is the hth interfering data symbol of the lth interferer, $p_l(t)$ is the transmit pulse of the lth interferer, τ_l is its delay, and $1/T_l$ its sample rate; $p_l(t)$ is assumed to be a square-root-raised cosine filter with roll-off α_l. The interfering signal is modulated to radio frequency $f_0 + f_{c,l}$, where $f_{c,l}$ is the carrier frequency deviation from f_0 for the lth interferer. The total NBI signal may

be seen at the output of the matched filter of the OFDM receiver as

$$r_I(t) = \sum_{l=1}^{N_I} \sum_{h=-\infty}^{\infty} b_{l,h}\, e^{j2\pi f_{c,l}hT_l}\, g_l(t - hT_l) \qquad (5)$$

where $g_l(t)$ is the convolution of $p_0(t)$ and $p_l(t - \tau_l)$ $\exp(j2\pi f_{c,l}t)$. It is assumed that the interfering symbols are uncorrelated with each other, i.e., $E[b_{l,h}b^*_{l',h'}] = E'_l \delta_{ll'}\delta_{hh'}$, where E'_l is the energy per symbol of the lth interferer. Further, the interfering data symbols $b_{l,h}$ are statistically independent of the OFDM data symbols a^i_k. The signal-to-interference ratio (SIR) at the input of the receiver is defined as

$$\text{SIR} = \frac{2\sigma_s^2/T_0}{\sum\limits_{l=1}^{N_I} \frac{E'_l}{T_l}}. \qquad (6)$$

III. STATISTICAL PROPERTIES OF THE TIMING METRIC IN THE PRESENCE OF NBI

In the S&C algorithm [1], the training symbol contains two identical halves in the time domain and the timing delay estimator searches for the peak of correlation between the matched filter output samples that are separated by half an OFDM symbol. The sample $r(mT_0)$ at the output of the matched filter of the OFDM receiver consists of a useful signal $r_u(mT_0)$, an interfering component $r_I(mT_0)$, and a noise component $w(mT_0)$. It may be expressed as

$$r(mT_0) = r_u(mT_0) + r_I(mT_0) + w(mT_0). \qquad (7)$$

The symbol timing estimator takes the instant d, where the timing metric

$$M(d) = \frac{|P(d)|^2}{R(d)^2} \qquad (8)$$

is maximum, as the starting point of the frame. In (8), $P(d)$ and $R(d)$ are given by

$$P(d) = \sum_{m=0}^{N/2-1} r^*\left((d+m)T_0\right) \cdot r\left(\left(d+m+\frac{N}{2}\right)T_0\right) \quad (9)$$

$$R(d) = \sum_{m=0}^{N/2-1} \left| r\left(\left(d+m+\frac{N}{2}\right)T_0\right)\right|^2. \qquad (10)$$

This timing metric is not only used to find the optimum timing instant, but also to determine whether or not a training sequence is received. To do this, we use a threshold: when the timing metric exceeds this threshold for at least one value of d, we decide that it is possible to detect a training sequence, whereas when the threshold is never exceeded, we decide that it is not possible to detect a training sequence. The value of the threshold must be selected such that the probability of missing a training symbol when there is one present, and the probability of falsely detecting a training sequence when there is none

present, are as small as possible. To find these probabilities, and hence the threshold, we need to know the statistical properties of the timing metric. In [1], the statistical properties of the timing metric at the optimum timing point and a position outside the training sequence were investigated. In this section, we extend the results of [1] to obtain the statistical properties of the timing metric in the presence of NBI.

First, we determine the mean of the timing metric in the presence of NBI signals as function of the timing position d. For sufficiently large values of SIR and SNR, $E\left[|P(d)|^2\right] \simeq |E[P(d)]|^2 \forall - (N/2+\nu) < d < N/2 - 1$: the imaginary part of $P(d)$ is small as compared with its real part and will be neglected. As the variances of $|P(d)|^2$ and $R(d)^2$ are small, $E[M(d)] \approx |E[P(d)]|^2/E[(R(d))^2]$, so that

$$E[M(d)] = \begin{cases} \dfrac{\left|2\cdot\sigma_s^2\left(d+\nu+\frac{N}{2}\right)+\psi\right|^2}{G^2}, & -\left(\frac{N}{2}+\nu\right) < d \le -\nu \\[2mm] \dfrac{\left|N\cdot\sigma_s^2+\psi\right|^2}{G^2}, & -\nu < d \le 0 \\[2mm] \dfrac{\left|2\cdot\sigma_s^2\left(-d+\frac{N}{2}\right)+\psi\right|^2}{G^2}, & 0 < d \le \frac{N}{2} - 1 \end{cases} \qquad (11)$$

where ψ and G are given by

$$\psi = \sum_{m=0}^{N/2-1} A^{(m,m)}\left(0, \frac{N}{2}\right) \qquad (12)$$

$$G = N\left(\sigma_s^2 + \sigma_n^2\right) + \sum_{m=0}^{N/2-1} A^{(m,m)}\left(\frac{N}{2}, \frac{N}{2}\right) \qquad (13)$$

and $A^{(m,m')}(x,y)$ is defined as

$$A^{(m,m')}(x,y) = \sum_{l=1}^{N_I} \sum_{h=-\infty}^{\infty} E'_l \cdot g^*_l\left((m+d+x)T_0 - hT_l\right)$$
$$\cdot g_l\left((m'+d+y)T_0 - hT_l\right). \quad (14)$$

When d is outside the region considered in (11), i.e., when $d \ge N/2$ or $d < -\nu - N/2$, the approximation $E\left[|P(d)|^2\right] \simeq |E[P(d)]|^2$ is no longer valid. However, it can easily be shown that in that case $E[M(d)] \simeq D^2/G^2$ (see also Section III-B), where D^2 is given by

$$D^2 = \frac{N}{2}\left(2\sigma_s^2 + 2\sigma_n^2\right)^2 + \sum_{m=0}^{N/2-1} A^{(m,m)}(0,0) \cdot A^{(m,m)}\left(\frac{N}{2}, \frac{N}{2}\right). \qquad (15)$$

In Section IV, we will evaluate the validity of the used approximations by means of simulations.

A. Optimum Timing Point

Let us define $q = |P(d_{\text{opt}})|/R(d_{\text{opt}})$ as the square root of the timing metric $M(d_{\text{opt}})$ at the optimum timing point d_{opt}. To simplify the notation, we drop the subscript "opt." Due to the symmetry of the pilot symbol, the signal component $\sum_{m=0}^{N/2-1} r^*_u((m+d)T_0) \cdot r_u((m+d+N/2)T_0)$ of $P(d)$ is real valued. It can easily be shown that the other components

of $P(d)$ have zero mean and small variance when the SIR and SNR are sufficiently large. Therefore, at high values of SNR and SIR, the imaginary part of $P(d)$ can be neglected. From (7), (9), and (10), it can easily be verified that $|P(d)|$ and $R(d)$ contain a common term α. Hence, we can rewrite $|P(d)|$ and $R(d)$ as $|P(d)| = \alpha + \beta$ and $R(d) = \alpha + \gamma$, where α, β, and γ, as well as their statistical properties, are given in the Appendix.

As can be observed in the Appendix, the expressions for α, β, and γ consist of a large number of contributions when N is large. Therefore, according to the central limit theorem, the variables α, β, and γ have approximate Gaussian distributions. Taking into account that for both the numerator and denominator of q, standard deviations are much smaller than the averages, q can be approximated by a Gaussian variable [14] with mean and variance given by the following approximations:

$$\mu_q \approx \frac{\mu_\alpha + \mu_\beta}{\mu_\alpha + \mu_\gamma} \tag{16}$$

$$\sigma_q^2 \approx \mu_q^2 \left(\frac{\sigma_\beta^2}{(\mu_\alpha + \mu_\beta)^2} + \frac{\sigma_\gamma^2}{(\mu_\alpha + \mu_\gamma)^2} \right) \tag{17}$$

where μ_x and σ_x^2 is the mean and variance of x, respectively. In (17), we have used the approximation $a(1 + b)/(1 + c) \simeq a(1 + b - c)$ as in [1]. Taking into account that q is approximately a Gaussian random variable, and $M(d)$ is the square of q, it follows that $M(d)$ also is approximately a Gaussian variable [14]:

$$M(d) = \left(\mu_q + N \left(0, \sigma_q^2 \right) \right)^2 \approx \mu_q^2 + 2 \cdot \mu_q \cdot N \left(0, \sigma_q^2 \right) \tag{18}$$

where $N(x, y)$ is a Gaussian random variable with mean x and variance y. The mean of $M(d)$, i.e., μ_M, can be easily computed calculated by using (16), as follows:

$$\mu_M = \left(\frac{N + \frac{1}{\sigma_s^2} \sum_{l=1}^{N_I} E_l' \Upsilon_l}{N + \frac{N}{\text{SNR}} + \frac{1}{\sigma_s^2} \sum_{l=1}^{N_I} E_l' \phi_l} \right)^2 \tag{19}$$

where Υ_l and ϕ_l are given as

$$\Upsilon_l = \text{Re} \sum_{m=0}^{N/2-1} \sum_{h=-\infty}^{\infty} g_l^*((m+d)T_0 - hT_l)$$
$$\cdot g_l \left(\left(m + d + \frac{N}{2} \right) T_1 - hT_l \right) \tag{20}$$

$$\phi_l = \sum_{m=0}^{N/2-1} \sum_{h=-\infty}^{\infty} \left| g_l \left(m + d + \frac{N}{2} \right) T_0 - hT_l \right|^2. \tag{21}$$

Note that (19) corresponds to the result in (11) for $d \in \,]-\nu, 0]$. Fig. 3 shows Υ_l and ϕ_l for one interferer ($N_I = 1$) as function of normalized interference frequency deviation, $\Gamma = f_{c,l}/((1 + \alpha_0)/2T_0)$. From Fig. 3, it follows that $\Upsilon_l \ll \phi_l$. It can easily be shown that when varying the normalized interference bandwidth (NBW) $= B_l/B_0$, where B_l is the bandwidth of lth interferer and B_0 is the bandwidth of OFDM signal; the same conclusions yield. Hence, the effect of the
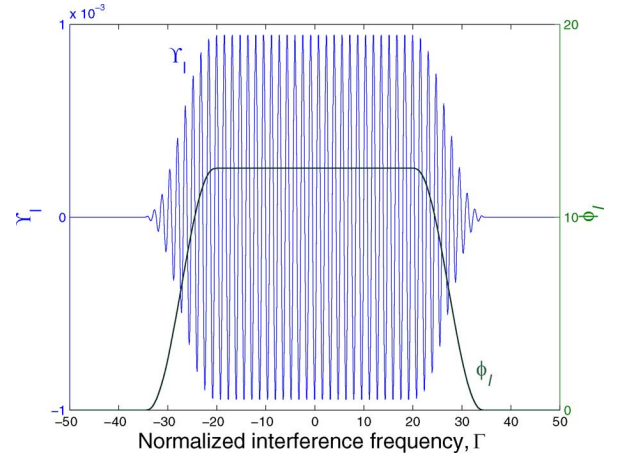

Fig. 3. Υ_l and ϕ_l (NBW $= 0.0244, N = 1024, \alpha_0 = .25, \alpha_l = .5$).

interference on the numerator of (19) will be much smaller than its effect on the denominator. Therefore, decreasing the SIR will result in a decrease of μ_M. When the interferer is located completely in the flat region of OFDM spectrum (see Fig. 2), i.e., $|f_{c,l} + (1 + \alpha_l)/2T_l| < ((1 - \alpha_0)/2T_0)$, $g_l(t)$ equals

$$g_l(t) = C \cdot p_l(t - \tau_l) \cdot e^{2\pi f_{c,l} t} \tag{22}$$

where C is constant. Using (22) in (20), Υ_l may be rewritten as

$$\Upsilon_l = C^2 \cdot \text{Re} \left\{ e^{j2\pi f_{c,l}(N/2)T_0} \sum_{m=0}^{N/2-1} \sum_{h=-\infty}^{\infty} p_l^* \left((m+d)T_0 - hT_l - \tau_l \right) \right.$$
$$\left. \cdot p_l \left(\left(m + d + \frac{N}{2} \right) T_0 - hT_l - \tau_l \right) \right\}. \tag{23}$$

Because of the factor $e^{j2\pi f_{c,l}(N/2)T_0}$ in (23), it follows that Υ_l is a periodic function of $f_{c,l}$ when the interferer is located in the flat region of the OFDM spectrum. Similarly, when we substitute (22) in (21), it turns out that ϕ_l becomes independent of $f_{c,l}$ in the flat region of the OFDM spectrum. This can be observed in Fig. 3.

According to (18), the variance of $M(d)$ is given by

$$\sigma_M^2 = 4 \cdot \mu_q^2 \cdot \sigma_q^2 \tag{24}$$

where σ_q^2 can be easily computed by using the (16) and (17). Note that, when SIR tends to infinity, the same expression for σ_M^2 is obtained as in [1].

B. Timing Position Outside of Training Sequence

In this section, the statistical properties of a timing position d outside of the training sequence are considered when NBI is present. Using a similar analysis as in [1], it can easily be verified that for sufficiently large SNR and SIR, the timing metric is approximated by a chi-square-distributed random variable, as follows:

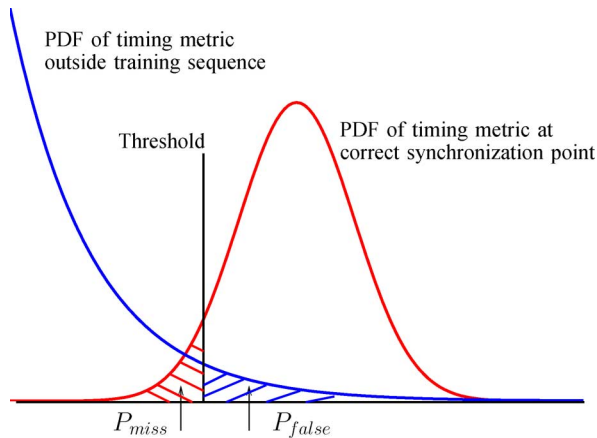$$M(d_{\text{outside}}) = \frac{D^2}{2G^2} \chi^2(2) \tag{25}$$

Fig. 4. Probability distributions of timing metric.

where $\chi^2(2)$ is a chi-square-distributed random variable with two degrees of freedom and its mean and variance equal to 2 and 4, respectively; G and D are given in (13) and (15), respectively. Therefore, the mean and the variance of $M(d_{\text{outside}})$ are given by

$$\mu_{M(d_{\text{outside}})} = \frac{D^2}{G^2} \tag{26}$$

$$\sigma^2_{M(d_{\text{outside}})} = \frac{D^4}{G^4}. \tag{27}$$

Note that these results are the same as in [1] when SIR tends to infinity.

C. Probability of Missing/False Detection of Training Sequence

In Fig. 4, the probability distributions of the timing metric are shown at the optimum timing instant and at an instant outside the training symbol as calculated in Sections III-A and III-B. These distributions can be used to determine both the probability of not detecting a training sequence when one is present, i.e., the probability of miss (P_{miss}), and the probability P_{false} of falsely detecting a training symbol when there is none present at a certain threshold value (λ). From the statistical communication theory, $P_{\text{miss}}(\lambda)$ and the probability $P_{\text{false}}(\lambda)$ are calculated as follows:

$$P_{\text{miss}}(\lambda) = .5 \operatorname{erfc}\left(\frac{\mu_M - \lambda}{\sqrt{2\sigma^2_M}}\right) \tag{28}$$

where $\operatorname{erfc}(x) = 2/(\sqrt{\pi}) \int_x^\infty e^{-z^2} dz$. Accordingly, $P_{\text{false}}(\lambda) = 1 - F(\lambda)$, where $F(\lambda)$ is the cumulative distribution function of a chi-square-distributed random variable with two degrees of freedom. The closed form of $F(\lambda)$ is obtained as [15]

$$F(\lambda) = 1 - e^{-\lambda/2\sigma^2_x} \tag{29}$$

where σ^2_x is the variance of i.i.d. Gaussian random variables, which equal $D^2/2G^2$ as in (25). Hence, $P_{\text{false}}(\lambda)$ can be written as

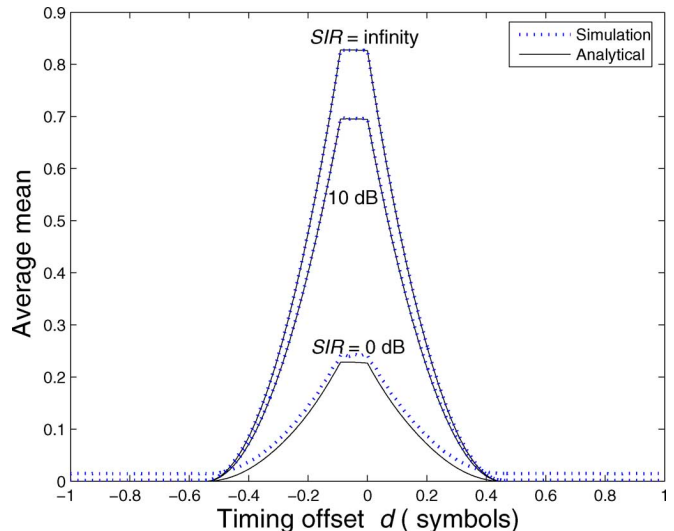$$P_{\text{false}}(\lambda) = e^{-\lambda G^2/D^2}. \tag{30}$$

Fig. 5. Average timing metric at SNR $= 10$ dB, NBW $= 0.0244$, $N_I = 1$, and $\Gamma = 0$.

IV. ANALYTICAL AND SIMULATION RESULTS

The numerical and simulation results in this paper are obtained with the following OFDM and interference parameters.[2]

- The total number of subcarriers is $N = 1024$.
- The total number of active subcarriers is $N_u = 1000$.
- The guard interval is set to about 10% of OFDM block size, $\nu = 102$.
- The bandwidth of the OFDM spectrum equals $B_0 = 1024$ kHz.
- We use QPSK modulation for the data symbols of the OFDM and the interferer signals.
- Transmit filters are square-root raised-cosine filters with roll-off factors $\alpha_0 = 0.25$ and $\alpha_l = 0.5$ for OFDM and interfering signals, respectively.
- Time delay of the interferers $\tau_l = 0$.

In [1], it is shown that the S&C timing algorithm is robust to fading channels. Therefore, we restrict our attention to an AWGN channel for simulation, to clearly show the effect of NBI on the performance of the synchronizer. However, the results of this paper can straightforwardly be extended to other types of channels.

In Fig. 5, the average timing metric based on the obtained analytical expression (11) is shown as function of the timing offset.[3] As can be observed, the timing metric shows a plateau at the maximum. This is explained as the cyclic prefix extends the symmetry of the OFDM pilot synchronization symbol such that all timing instants within the cyclic prefix will give rise to the same timing metric. This plateau will result in an ambiguity in the selection of the optimum timing. However, a timing offset within the cyclic prefix will cause no interference but only

[2]For the sake of comparison between our results and results presented in [1], we use the same parameters as in [1]. However, in the actual hardware implementation, the number of null subcarriers would be higher to ease filtering requirements. Moreover, the analysis of the paper is valid for other antialiasing filters than square-root raised-cosine filter; one just has to plug in the correct expression for these filters in our equations.

[3]It is easy to verify that if the normalized selective channel is considered, we obtain the same average timing metric.
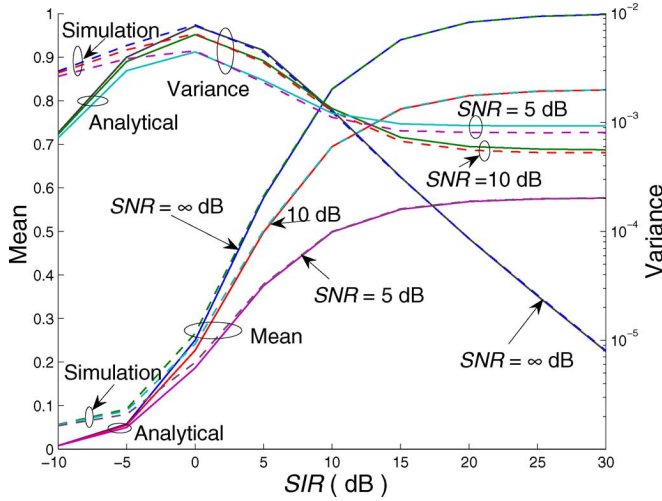
Fig. 6. Mean and variance of timing metric at optimum point (NBW = 0.0244, $N_I = 1$, and $\Gamma = 0$).

Fig. 7. Mean and variance of timing metric at optimum point (SNR = 10 dB, $N_I = 1$, and $\Gamma = 0$).

Fig. 8. Mean and variance of timing metric at optimum point (SNR = 10 dB, $N_I = 1$, and NBW = 0.0244).

gives rise to a carrier-dependent phase rotation at the fast Fourier transform (FFT) output, which can easily be compensated by the equalizers. Further, simulation results on the average timing metric are shown. As can be observed, the analytical results well correspond with the simulation results. Only at very low SIR, the analytical curve starts to deviate slightly from the simulation results: for very small SIR, the approximations used in the theoretical analysis are no longer valid. The narrowband interference causes a decrease of the maximum of the timing metric when the SIR decreases, i.e., when the power of the interferer increases. As a result, the risk that the timing metric will not exceed the threshold will increase such that the probability that the receiver will conclude that there is no training symbol present will increase.

Fig. 6 shows results for the mean and variance of the timing metric at the optimum timing instant, as function of the SIR. For a large range of SIR, the theoretical results and the simulation results agree well. At large SIR, the mean of the timing metric reaches an asymptote, corresponding to the case where no interference is present. This asymptote depends only on the SNR and is given by $(1 + 1/\text{SNR})^{-2}$. At very low SIR, the mean of the timing metric becomes independent of the SNR. The theoretical results give rise to a maximum timing metric that is smaller than for the simulations when the SIR is small. Hence, the theoretical results can be considered as a lower bound on the performance for small SIR. The variance of the timing metric decreases for increasing SIR. This can easily be explained as at high SIR and SNR, the effect of the noise and interference is small, such that the symmetry of the pilot symbol is almost not affected, and the timing metric will be close to its average.

Fig. 7 shows results for the mean and variance of the metric at the optimum timing point as function of the interference bandwidth. The results indicate that at given SIR, the mean is independent of the interference bandwidth. Further, the dependency of the variance on the interference bandwidth increases when SIR decreases. This is explained as at high SIR, the effect of interference diminishes and the variance mainly depends on noise.
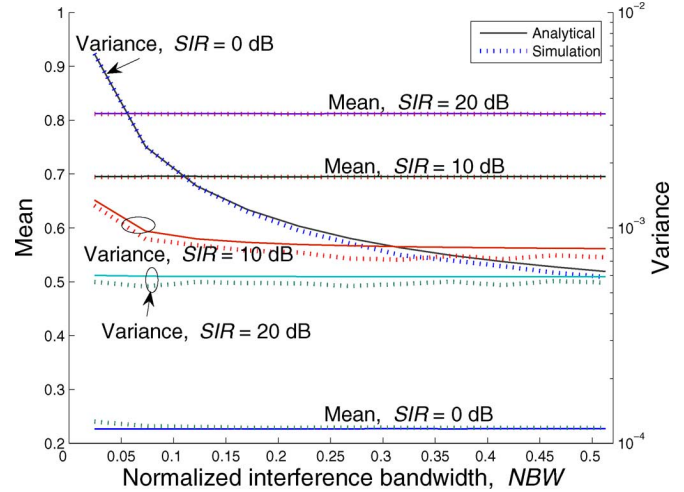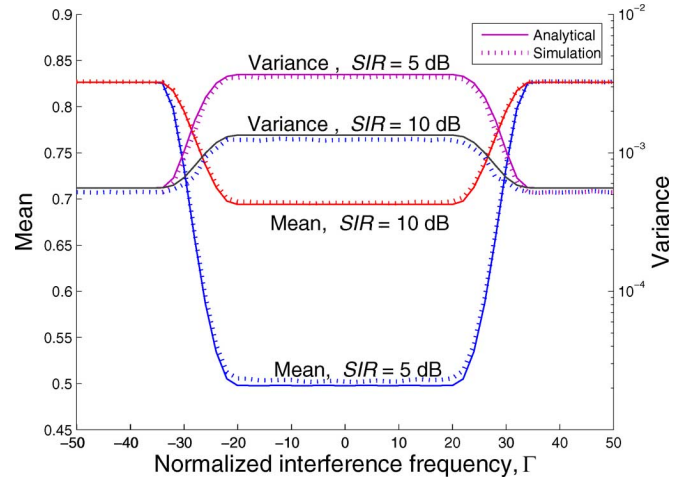
At low SIR, the variance decreases when the interference bandwidth increases.

Fig. 8 illustrates results for the mean and variance of the timing metric at the optimum timing point as function of the normalized interference carrier frequency deviation Γ. The shape of the mean may be explained with the aid of Fig. 2. As long as the interfering signal is located in the flat region of the OFDM spectrum, i.e., $|\Gamma + ((1 + \alpha_l)/(1 + \alpha_0))(T_0/T_l)| < ((1 - \alpha_0)/(1 + \alpha_0))$, the mean is constant and does not depend on Γ. When the interfering signal is located outside OFDM bandwidth, i.e., $(\Gamma + ((1 + \alpha_l)/(1 + \alpha_0))(T_0/T_l) > 1$ or $\Gamma - ((1 + \alpha_l)/(1 + \alpha_0))(T_0/T_l) < -1)$, the interfering signal does not affect the OFDM signal anymore: in this region the mean is constant and its value depends on the SNR value only. The periodicity of Υ_l (see Fig. 3) does not appear in Fig. 8 because Υ_l is much smaller than ϕ_l. Therefore, the contribution of Υ_l on the mean and variance of the timing metric can be neglected.
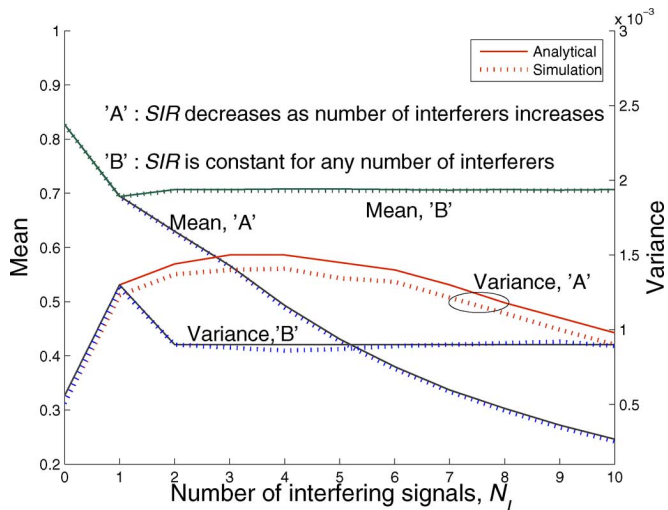
Fig. 9. Mean and variance of timing metric at optimum point (SNR $= 10$ dB, SIR $= 10$ dB, NBW $= 0.0244$, and $\Gamma = 0$).
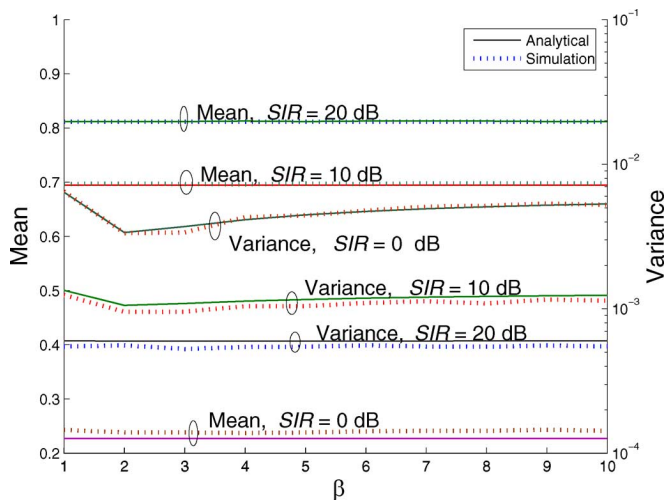

Fig. 11. Mean and variance of timing metric outside training sequence at (SNR $= 10$ dB, NBW $= 0.0244$, $\Gamma = 0$, and $N_I = 1$).

Fig. 10. Mean and variance of timing metric at optimum point at (SNR $= 10$ dB, $N_I = 2$, NBW $= 0.0244$, and $\Gamma = 0$).

Fig. 12. Probability of missing a training sequence ($\lambda = 0.4$, NBW $= 0.0244$, and $\Gamma = 0$, $N_I = 1$).

Fig. 9 shows the mean and the variance of the timing metric at the optimum synchronization point as function of the number of interfering signals, N_I, in two cases. In case "A," we consider that the SIR is fixed per interferer, so the total SIR decreases inversely proportional to N_I. In case "B," we consider a fixed total SIR, i.e., SIR per interferer decreases linearly as N_I increases. As the mean and variance mainly depends on the total SIR, it follows that the mean and variance will be decreasing functions of the number N_I of interferers in case "A," whereas they are independent of N_I in case "B."

Let us consider the case of two interferers ($N_I = 2$). We define the SIR for the first interferer (SIR$_1$) as $\beta \cdot$ SIR. Noting that (6) may be rewritten as SIR $= 1/\sum_{i=1}^{N_I} 1/\text{SIR}_i$, where SIR$_i = ((2\sigma_s^2/T_0)/(E_i/T_i))$, the SIR for the second interferer (SIR$_2$) is SIR$/(1 - 1/\beta)$. Fig. 10 shows the mean and the variance of the timing metric at the optimum synchronization point as function of β. The results indicate that the statistical properties of the timing metric at the optimum timing point do not depend on SIR per interferer but only depend on the total SIR.
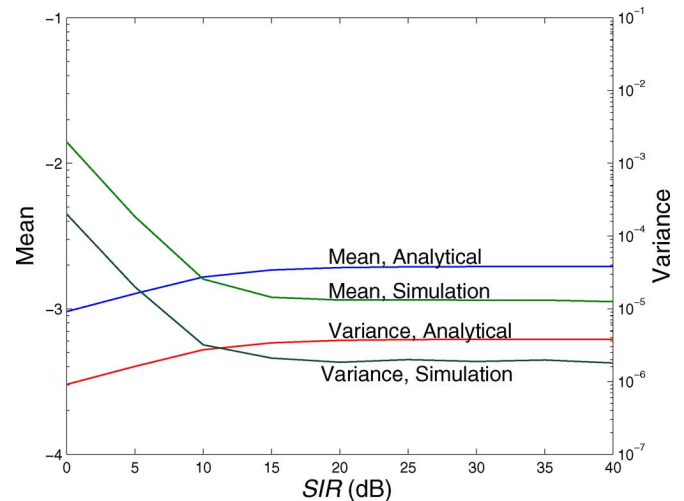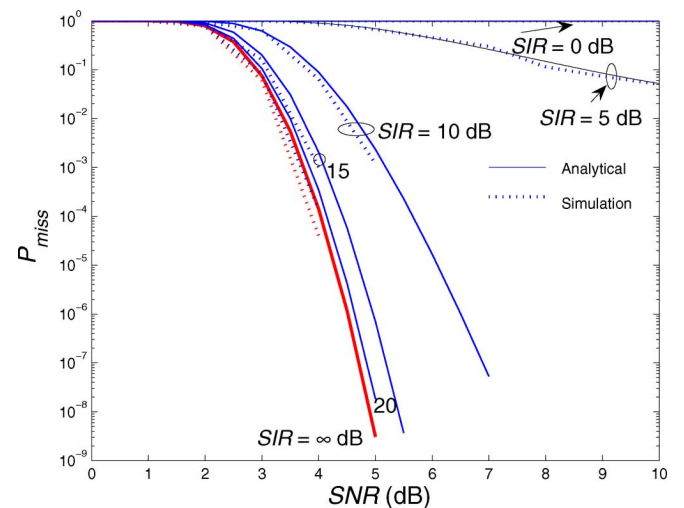
Fig. 11 illustrates the results for the mean and variance of the timing metric at a timing instant *outside* the training symbol as function of SIR. At high SIR values, the interference signal does not affect the statistical properties of timing metric outside training symbol. Note that the simulation results are slightly different from the analytical results. This is caused by correlations between the signal terms $r^*((m+d)T_0)$ and $r((m+d+N/2)T_0)$ outside the training symbol, while the theoretical analysis assumed that they were independent.

Fig. 12 displays the results for the probability of missing a training sequence P_{miss} at threshold $\lambda = 0.4$.[4] The results show that P_{miss} strongly depends on the NBI signal when the SIR is less than 15 dB. This is explained as the NBI signal destroys the correlation between the two halves of the received pilot sequence.

On the other hand, Fig. 13 illustrates the analytical results of the probability of false detection P_{false} as a function of SNR at

---

[4]The threshold level should be adapted according to the desired probability of missing a training sequence and probability of false detection.
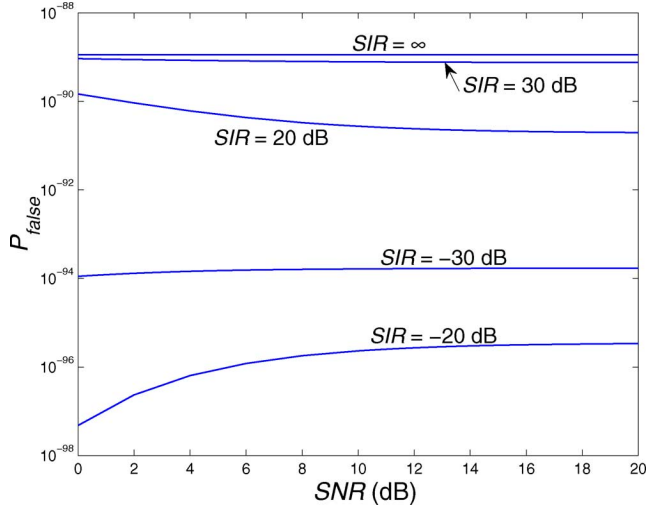
Fig. 13. Probability of false detecting a training sequence ($\lambda = 0.4$, NBW $= 0.0244$, $\Gamma = 0$, and $N_I = 1$).

different values of SIR. Note that at SIR $= \infty$ dB, the chi-square distribution is not a function of SNR, but only of the length of the training sequence. This explains why P_{false} is independent of the SNR at SIR $= \infty$ dB. Further, the values of P_{false} are very small, approximately equal to zero. This can be explained as the length of the correlation ($N = 1024$) is large enough to cancel out the effect of noise, OFDM data, and the NBI signal. It is clear from the figure that the probability of a false detection is too small to be checked by computer simulations.

V. CONCLUSION

This paper evaluates the performance of the S&C symbol timing estimator [1] in the presence of narrowband interference for different interference signal parameters. The statistical properties of the estimator are evaluated analytically and by means of simulation at the optimum synchronization point and outside the training sequence. Further, the probabilities of both missing and false detection of the training sequence are investigated. The agreement between the theoretical and simulation results proves the validity of our analysis. Generally, results indicate that the estimator works well for a wide range of SIRs. Also, at high SIR values (≥ 10 dB), noise is the dominant factor on the statistical properties of the estimator. Furthermore, at a given value of SIR, the interference bandwidth does not influence the mean of the metric while the dependency of the variance of the metric on the interferer bandwidth increases when SIR decreases. Moreover, the interference carrier frequency deviation does not affect the statistical properties of the estimator as long as the interferer is located in the flat region of the OFDM spectrum. The statistical properties of the estimator at optimum timing point do not depend on the SIR per interferer but only depend on the total SIR. At high values of SIR, the statistical properties of the estimator at a position outside the training symbol are essentially independent of the interference signal. Moreover, the probability of missing a training symbol is strongly affected by NBI as long as SIR is less than 15 dB. Finally, the probability of false detection approximately equals zero independent of the value of SNR and SIR.

APPENDIX

α, β, and γ may be written as

$$\alpha = \sum_{m=0}^{N/2-1} \{\text{Re}\{r_u^*(z_m)\, r(y_m)\} + jIm\{r_u^*(z_m)\, r_u(y_m)\}\} \quad (31)$$

where $z_m = (m+d)T_0$ and $y_m = (m+d+N/2)T_0$.

$$\beta = \sum_{m=0}^{N/2-1} \text{Re}\{(r_I^*(z_m) + w(z_m))\, r(y_m)\} \quad (32)$$

$$\gamma = \sum_{m=0}^{N/2-1} \text{Re}\{(r_I^*(y_m) + w^*(y_m))\, r_u(y_m)\}$$

$$+ 2 \cdot \text{Re} \sum_{m=0}^{N/2-1} r_I^*(y_m) \cdot w(y_m)$$

$$+ \sum_{m=0}^{N/2-1} \{|w(y_m)|^2 + |r_I(y_m)|^2\}. \quad (33)$$

After tedious computations, it follows that the mean and variance of α, β and γ can be written as

$$\mu_\alpha = N \cdot \sigma_s^2 \quad (34)$$

$$\mu_\beta = \text{Re} \sum_{m=0}^{N/2-1} A^{(m,m')}\left(0, \frac{N}{2}\right) \quad (35)$$

$$\sigma_\beta^2 = \sum_{m=0}^{N/2-1} \left\{(\sigma_s^2 + \sigma_n^2)\, A^{(m,m)}(0,0) + \sigma_n^2 A^{(m,m)}\left(\frac{N}{2}, \frac{N}{2}\right)\right\}$$

$$+ N \cdot \sigma_n^2 \cdot (\sigma_s^2 + \sigma_n^2)$$

$$+ 0.5 \sum_{m,m'=0}^{N/2-1} A^{(m,m')}(0,0) \cdot \left(A^{(m,m')}\left(\frac{N}{2}, \frac{N}{2}\right)\right)^* \quad (36)$$

$$\mu_\gamma = N \cdot \sigma_n^2 + \sum_{m=0}^{N/2-1} A^{(m,m)}\left(\frac{N}{2}, \frac{N}{2}\right) \quad (37)$$

$$\sigma_\gamma^2 = (\sigma_s^2 + 4\sigma_n^2) \sum_{m=0}^{N/2-1} A^{(m,m)}\left(\frac{N}{2}, \frac{N}{2}\right)$$

$$+ N.\sigma_n^2 (\sigma_s^2 + 2\sigma_n^2)$$

$$+ \sum_{m,m'=0}^{N/2-1} \left(A^{(m',m)}\left(\frac{N}{2}, \frac{N}{2}\right)\right)^* \cdot \left(A^{(m,m')}\left(\frac{N}{2}, \frac{N}{2}\right)\right)^*$$

$$- \sum_{m,m'=0}^{N/2-1} B^{(m,m')}\left(\frac{N}{2}, \frac{N}{2}\right) \quad (38)$$

where $B^{(m,m')}(x,y)$ is given by

$$B^{(m,m')}(x,y) = \sum_{l=1}^{N_I} \sum_{h=-\infty}^{\infty} (E_l')^2 \cdot |g_l((m+d+x)T_0 - hT_l)|^2$$

$$\cdot |g_l((m'+d+y)T_0 - hT_l)|^2. \quad (39)$$

REFERENCES

[1] T. Schmidl and D. Cox, "Robust frequency and timing synchronization for OFDM," *IEEE Trans. Commun.*, vol. 45, no. 12, pp. 1613–1621, Dec. 1997.

[2] J. Zander, "Radio resource management in the future wireless networks: Requirements and limitations," *IEEE Commun. Mag.*, vol. 35, no. 8, pp. 30–36, Aug. 1997.

[3] J. Mitola, "Cognitive radio for flexible mobile multimedia communications," presented at the IEEE Int. Workshop Mobile Multimedia Communications, San Diego, CA, Nov. 1999.

[4] M. Schnell, "B-VHF—An overlay system concept for future ATC communications in the VHF band," presented at the 23rd Digital Avionics Systems Conf. (DASC), Salt Lake City, UT, Oct. 2004.

[5] B. Haindl *et al.*, "B-VHF—A multi-carrier based broadband VHF communications concept for air traffic management," in *Proc. IEEE Aerosp. Conf.*, Big Sky, MT, Mar. 2005, pp. 1894–1904.

[6] A. J. Coulson, "Narrow band interference in pilot symbol assisted OFDM systems," *IEEE J. Sel. Areas Commun.*, vol. 3, no. 6, pp. 2277–2287, Nov. 2004.

[7] K. Witrisal, "OFDM air-interface design for multimedia communications," Ph.D. dissertation, Electrical Eng. Dept., Delft Univ. of Technology, Delft, The Netherlands, 2002.

[8] M. Marey and H. Steendam, "The effect of narrowband interference on frequency ambiguity resolution for OFDM," presented at the Vehicular Technology Conf. (VTC) Fall 2006, Montréal, QC, Canada, Sep. 2006.

[9] J. A. C. Bingham, "Multicarrier modulation for data transmission: An idea whose time has come," *IEEE Commun. Mag.*, vol. 28, no. 5, pp. 5–14, 1990.

[10] K. Fazel and S. Kaiser, *Multi-Carrier and Spread Spectrum Systems*. New York: Wiley, 2003.

[11] I. Kalet, "The multitone channel," *IEEE Trans. Commun.*, vol. 37, no. 2, pp. 119–124, Feb. 1989.

[12] H. Minn, V. Bhargava, and K. Lataief, "A robust timing and frequency synchronization for OFDM systems," *IEEE Trans. Wireless Comun.*, vol. 2, no. 4, pp. 822–838, Jul. 2003.

[13] A. J. Coulson, "Maximum likelihood synchronization for OFDM using a pilot symbol: Algorithms," *IEEE J. Sel. Areas Commun.*, vol. 19, no. 12, pp. 2486–2494, Dec. 2001.

[14] R. Walpole and R. Myers, *Probability and Statistics for Engineers and Scientists*, 5th ed.   Englewood Cliffs, NJ: Prentice-Hall, 1993.

[15] J. G. Proakis, *Digital Communications*, 3rd ed.   New York: McGraw-Hill, 1995.

Mohamed Marey received the B.Sc. and M.Sc. degrees in electrical engineering from Menoufyia University, Menouf, Egypt, in 1995 and 1999, respectively. He is currently working towards the Ph.D. degree at the Department of Telecommunications and Information Processing (TELIN), Ghent University, Gent, Belgium, for which he was granted a fund for scientific research from the government of the Arab Republic of Egypt in 2004.

Previously, he worked as an instructor and Assistant Lecturer in the Department of Electronic and Communication Engineering, Menoufyia University, from 1996 to 1999 and 1999 to 2004, respectively. His main research interests include synchronization, channel estimation, coding, and interference cancellation for wireless multicarrier communication systems. He is the author of several scientific papers.

Mr. Marey received the Young Scientist Award from the International Union of Radio Science (URSI) in 1999.

Heidi Steendam (M'01–SM'05) received the M.Sc. degree in electrical engineering and the Ph.D. degree in applied sciences from Ghent University, Gent, Belgium, in 1995 and 2000, respectively.

Since September 1995, she has been with the Digital Communications (DIGCOM) Research Group, Department of Telecommunications and Information Processing (TELIN), Faculty of Engineering, Ghent University, first in the framework of various research projects, and since October 2002 as a full-time Professor in the area of digital communications. She is teaching courses on data communications, information theory, and advanced modulation and coding techniques. Her main research interests are in statistical communication theory, carrier and symbol synchronization, bandwidth-efficient modulation and coding, spread-spectrum (multicarrier spread-spectrum), satellite, and mobile communication. She is the author of more than 80 scientific papers in international journals and conference proceedings.

Dr. Steendam has been active in various international conferences as Technical Program Committee Member and Session Chair. Since 2002, she has been an Executive Committee Member of the IEEE Communications and Vehicular Technology Society Joint Chapter, Benelux Section. In 2004, she was the conference chair of the IEEE Symposium on Communications and Vehicular Technology in the Benelux Section.